Bridge Structures 6 (2010) 3–24
DOI:10.3233/BRS-2010-005
IOS Press

Performance and operational allowable speed limit for vehicles on cable stayed bridges

Ben Y.B. Chan* and Moe M.S. Cheung
Department of Civil and Environmental Engineering, The Hong Kong University of Science and Technology, Hong Kong, P.R. China

Abstract. The ever increasing numbers of fatal vehicle accidents worldwide on cable-stayed bridges under serviceable wind conditions, has rung the alarm bells for engineers to consider the safety issue in an operation level. The new generation of structural designs also involves the efficient and comfortable use of the structure by the end user. When this 'design for the user' concept is applied to bridges, investigation of vehicles travelling on long span bridges subjected to strong wind attacks not only allows the designer to have more understanding about the actual performance of a bridge at the operation level, but the safety and comfort of the drivers can also be studied. However, reliability analysis on a vehicle-bridge-wind system is such a time consuming process that it is usually considered infeasible in actual practice, especially when dealing with highly non-linear cable-stayed bridges.

This study has constructed a general, yet efficient, vehicle stability analysis framework which makes possible the estimation of the maximum allowable vehicle velocity on cable-stayed-bridges subjected to different wind intensities. Non-linear properties such as the cable sag, geometrical non-linearity and wind induced buffeting and fluttering effects are studied and implemented into the analysis framework. In addition, the numerical simulation procedure is optimized using the partial iterative process (PIP) and the continuous simulation technique (CST), which can significantly reduce the time needed for performing the reliability analysis. The result of the numerical example demonstrated that both high-sided vehicles and small vehicles are likely to undergo vehicle instability problems on cable-stayed bridges subjected to wind loading. It is also suggested that the allowable speed limit for vehicle travelling on cable-stayed bridges are significantly lower than the limit on box-girder bridges. Besides, under serviceable wind loadings, the stability of a vehicle depends very much on the speed of vehicle, the roughness conditions on the deck and the degree of the coupling effect between the bridge and the vehicle.

Keywords: Reliability analysis, vehicle stability, cable-stayed bridge, operational requirement, wind effect

1. Introduction

The cable stayed bridge was introduced in the 1600s when the Venetian engineer Verantius sketched a bridge with several diagonal chain stays in his book. Nowadays, the cable-stay bridge is generally defined as a structural system which comprises a continuous deck system which is supported by stays, i.e. inclined cables passing over or attached to towers located at the main piers. In 1949, the German engineer F. Dischinger recognized that the cables of early cable stay bridges were never subject to any initial tension which resulted in unacceptably flexible behaviour. Thereafter, the development and application of electronic computers opened up new and practically unlimited possibilities for the exact solution of these highly statically indeterminate systems and for precise statical analysis of their three-dimensional performance. Moreover, with the introduction of high-strength steels, orthotropic type decks, the development of welding techniques and progress in structural analysis, various concerns regarding the construction of cable stay bridges have been overcome.

*Corresponding author. Ben Y.B. Chan, Department of Civil and Environmental Engineering, The Hong Kong University of Science and Technology, Clear Water Bay, Hong Kong, P.R. China. Tel.: +852 2358 8721; Fax: +852 2358 1534; E-mail: ybchan@ust.hk.

Owing to a better understanding of the behaviour and performance of cable-stayed bridges, bridge engineers now recognize the many advantages of this type of bridge in terms of economy, ease of fabrication and construction, aesthetics and the various possibilities for structural arrangements, etc. Nowadays, cable-stayed bridge has been widely recognized as a very efficient and competitive type of bridge, with spans ranging 200 m to 800 m. The recent trend of having very long span lengths is quite remarkable in the design of this kind of bridge. Because of the long span length, modern cable-stayed bridges have lower stiffness and mechanical damping properties than bridges of more typical span lengths, which results in a more flexible structural system. The behaviour of such long-span cable-stayed bridges, subjected to dynamic load conditions caused by vehicles, earthquakes and severe wind, is of great interest of engineers and researchers.

While the structural stability of cable-stayed bridges is well secured, through the improvement of design codes and regulations, the safety of the drivers and the stability of the vehicles travelling on these flexible structures have not been seriously addressed to. In recent years, there have been increasing reports regarding fatal vehicle accidents on cable-stayed bridges during strong wind events [7, 19]. Besides, it has also been reported that high-sided vehicles can slide and even overturn under strong wind gusts [14, 21, 22].

In order to secure the safety of bridge users, it is necessary to understand the performance of vehicles on cable-stayed bridges subjected to severe wind attacks. Furthermore, the investigation of vehicles travelling on cable-stayed bridges under wind loading not only allows the designer to have a better understanding of the actual performance of a bridge at the operation level, but it also enhances the serviceability of the structure in terms of safety and drive comfort. The outcome of such investigation leads to the improvement of the design codes and the development of some operational criteria to better suit the needs of the drivers, including a higher level of comfort, a shorter travelling time and a higher driving safety assurance.

Although the potential value of predicting the maximum allowable driving speed on long span bridges has been well accepted, there is very little information in this area, and a complete and efficient solution to this problem is as yet unavailable. The fact is that the complexity and randomness of this problem make it very difficult to provide a general solution. Complexity comes from the coupled relationship between the wind, the vehicles and the non-linear behavior of the flexible cable-stayed structure. The response of a vehicle depends very much on the wind forces and the motion of the vehicle. On the other hand, the motion of the vehicle itself can be treated as an external force acting on the bridge which alters the already-complex non-linear motion of the cable-stayed system. These interactions are coupled which makes it impossible to use a quasi-static approach for the solution. Furthermore, it has been generally accepted that wind is random in nature, and it is very difficult to accurately model a wind event without simplification. In saying that wind is very difficult to model, it is even more difficult to predict the random response of long span structures, which are prone to wind induced excitation problems, not to mention the fact that the responses of two coupled bodies, the vehicle and the bridge, have to be predicted. Moreover, with the random responses obtained from the random driving forces, a general conclusion on the responses is not possible without a huge amount of data.

In the early studies of wind generated responses of structures, the wind actions were approximated as static forces caused by the wind pressure. It was not until the collapse of the Tacoma Narrows Bridge under a wind condition of only moderate intensity of 19 m/s on November 7, 1940, did the engineers realize the importance of the dynamic effects of the wind loads on the structures. Therefore, in the study of the dynamic effects on cable-stayed bridges, the wind induced vibration and cross-wind excitations should be carefully considered.

Vehicle-bridge interaction (VBI) is the term decrypting the coupled interaction between the bridge and vehicle and has been vigorously developed in the past few decades. Yang et al. [25] and Yang and Lin [24] gave a very detailed review on the early development of such interaction problems. With advancements in the use of the Finite Element Method (FEM) and high-performance computers, more realistic bridge and vehicle models have been developed. Xu and Guo [21, 22] developed a 7-degrees-of-freedom vehicle model, with three body masses representing the main vehicle mass, the front axis mass and the rear axis mass. Each of the masses is connected by spring-dashpot systems and pivots to account for the elasticity and energy dissipating characteristics. With the FE vehicle and bridge model, the coupling forces between the vehicle system and the bridge system can be determined by iterative searching, but the extremely slow convergence rate, due to its iterative nature, makes the vehicle-bridge interaction analysis very difficult, if not impossible, to apply in real practice. Yang developed a "VBI Element" in

1995 for dynamic analysis of vehicle-bridge interaction problems. Yang combined the vehicle system and the bridge system using VBI Elements and solved the characteristic equations of both systems interactively in Lagrangian formulation. Recently, researchers such as Cai and Chen [4] and Xu and Guo [22] investigated the wind induced effect and crosswind responses on high-sided vehicles, with consideration of the sharp-edged wind fields. Moreover, Chen and Cai [7] and Guo and Xu [13] further extended their studies on the safety issue and concluded that high-sided vehicles can overturn on bridges under strong winds, and that the safety of vehicles mainly depends on wind and vehicle velocities. In addition, by re-defining the vehicle instability criteria, the authors of this paper [8] investigated an integrated approach to simulation of the vehicle performance on a continuous bridge subjected to some simulated wind events and estimated the operational speed limit for vehicles travelling on box-girder bridges.

However, these approaches are either too specific or only good enough for normal continuous slab-on-girder bridges. In this regard, the research reported in this paper tried to implement the innovative vehicle stability analysis technique to cable-stayed bridges, with consideration of the wind induced excitation mechanisms and the non-linear behaviour of the cable-stays and the deck.

2. Formulation of vehicle-wind-cable stayed bridge interaction model

This study adopted the concept of the integrated Vehicle Performance Simulation (VPSIM) framework developed by the authors in 2008 to predict the optimum allowable vehicle speed limit on cable-stayed bridges under different intensities of wind loading, by constructing and solving the non-linear characteristic equation of motion of the coupled vehicle-wind-bridge system. To implement the cable sag and wind induced flutter effect, the iterative algorithm for non-linearity is combined with the direct integration algorithm for time domain simulation.

The integrated framework proposed by Cheung and Chan is a real-time simulation and monitoring procedure, which includes an interactive, dynamic vehicle performance simulation module and a real-time stepwise vehicle stability assessment module. Figure 1 graphically demonstrates the components and major interaction considerations of the simulation module. The vehicle model is simplified as a combination of rigid masses connected by a series of springs and damping devices with seven degrees-of-freedom. Besides, classical Rayleigh damping is assumed for both the vehicle and the bridge models. To generate the correlated road roughness and wind velocity fields, the classical spectral representation method introduced by Shinozuka and Deodatis [17] is adopted. Assuming a power spectral density (PSD) at a constant vehicle velocity, the correlated road roughness profile $r(x_2)$ corresponds to the independent line of roughness $r(x)$ and can be generated as follows:

$$r(x_2) = \sum_{i=1}^{N} \gamma_{xy}(f_i)\sqrt{4S(f_i)\Delta f}\cos(2\pi f_i x + \theta_i) + \sum_{i=1}^{N} \sqrt{1-\gamma_{xy}^2(f_i)}\sqrt{4S(f_i)\Delta f}\cos(2\pi f_i x + \phi_i) \tag{1}$$

where N is a sufficiently large number; f_i is the circular frequency within the interval in which the PSD is defined; $S(f_i)$ is the cross-spectrum density component at frequency f_i ; x is the distance from the initial point and θ_i is the random phase angle uniformly distributed from 0 to 2π; Δf is defined as the frequency increment, where $\Delta f = (f_{up})/N$; $\gamma_{xy}(f_i)$ is the coherence function, which can be calculated using the procedure presented by Liu [15].

For the wind velocity field, Cao et al. [5] suggested that the orthogonal wind velocity spectrum is very small in the atmosphere and can be omitted. In such cases,

$$F_j(t) = \sqrt{2(\Delta\omega)}\sum_{m=1}^{j}\sum_{l=1}^{N}\sqrt{S(\omega)}G_{jm}(\omega_{ml}) \times \cos(\omega_{ml}t + \phi_{ml}) \tag{2}$$

where ω represents the frequency; N is a sufficiently large number; Φ_{ml} is the random phase angle, distributed uniformly from 0 to 2π; $S(\omega)$ is the cross-spectral density matrix; $G_{jm}(\omega_{ml})$ is determined from the mathematical induction of $H(\omega)$ and is defined by:

$$G(\omega) = \begin{bmatrix} 1 & 0 & 0 & \cdots & 0 \\ C & \sqrt{1-C^2} & 0 & \cdots & 0 \\ C^2 & C\sqrt{1-C^2} & \sqrt{1-C^2} & \cdots & 0 \\ \vdots & \vdots & \vdots & \ddots & \vdots \\ C^{n-1} & C^{n-2}\sqrt{1-C^2} & C^{n-3}\sqrt{1-C^2} & \cdots & \sqrt{1-C^2} \end{bmatrix} \tag{3}$$

with

$$C = \exp\left(-\frac{\lambda\omega\Delta}{2\pi U(z)}\right) \tag{4}$$

By resolving the vehicle system in terms of the interaction forces, and substituting it into the bridge system, Cheung and Chan [8] demonstrated that the characteristic equation of motion of the coupled system can be constructed in the following form:

$$\begin{bmatrix} [m_v] & \langle 0\rangle \\ \{0\} & [m_b] \end{bmatrix} \begin{Bmatrix} \{\ddot{v}_v\} \\ \{\ddot{v}_b\} \end{Bmatrix} + [C_{vb}] \begin{Bmatrix} \{\dot{v}_v\} \\ \{\dot{v}_b\} \end{Bmatrix} + [K_{vb}] \begin{Bmatrix} \{v_v\} \\ \{v_b\} \end{Bmatrix} = \begin{Bmatrix} \{f_{wind\_v}\} \\ \{f_{wind\_b}\} \end{Bmatrix} \tag{5}$$

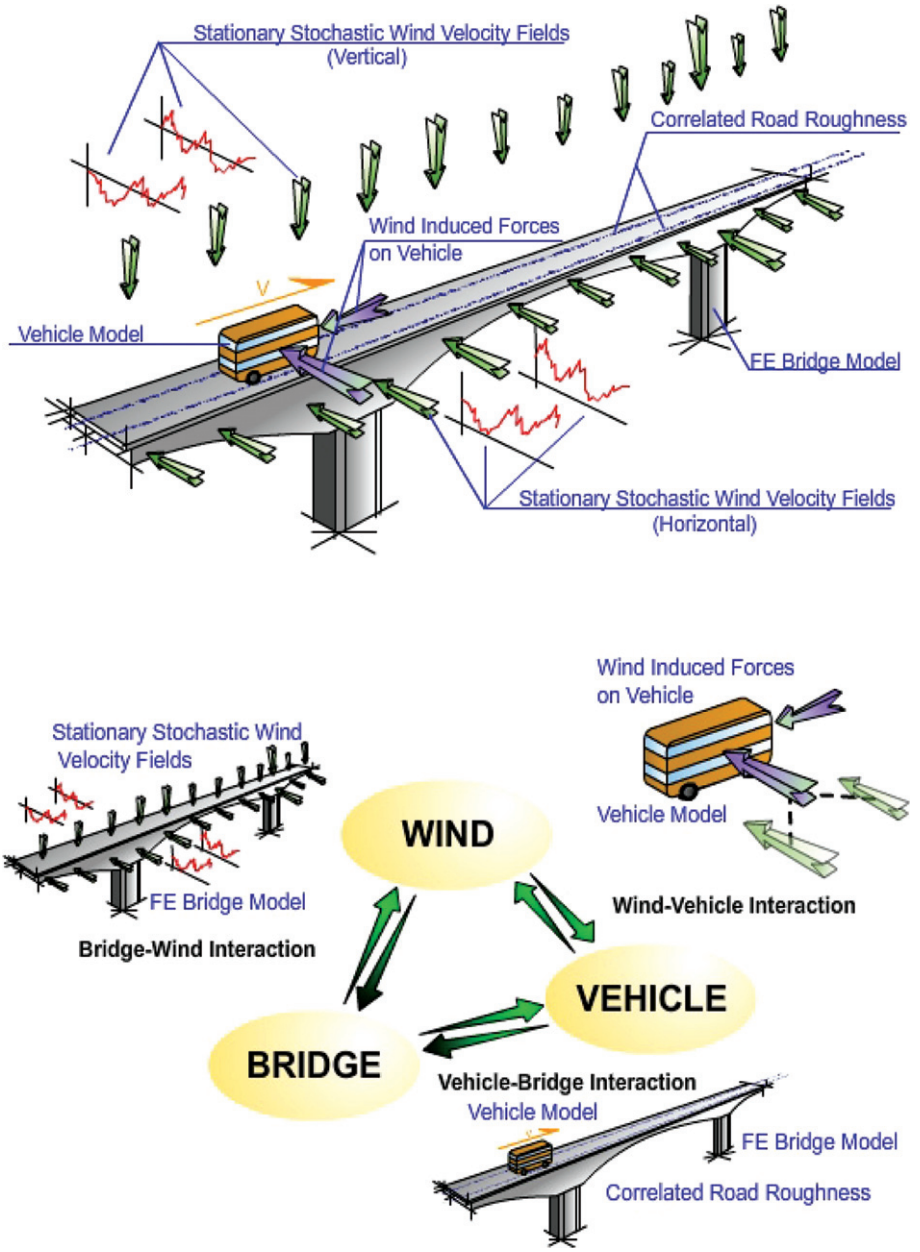

Fig. 1. Vehicle-wind-bridge interactions model.

where $[C_{vb}]$ and $[K_{vb}]$ are the coupled damping and stiffness matrices, which change with the position of the vehicle. Equation 5 can be considered as an ordinary differential equation of two variables, time and position. It can be solved numerically using a direct integration based simulation technique to simulate the vibration of the coupled system, with consideration of the vehicle-wind-bridge interactions.

When the vehicle stability analysis framework is applied to the cable-stayed bridge, two major obstacles are presented. First of all, the proposed method requires the extraction of the mass, the stiffness and damping matrices from the FEM model to construct the coupled characteristic equations of motion. This method is applicable only when all the elements are linear elastic elements. However, the non-linearity of the cables cannot be ignored as it governs the vibration of the whole structure. Although many finite elements packages, including ANSYS, allow the assignment of non-linear cable elements during the model construction stage, the non-linear property of the cables is lost when extracting the matrices information out of these packages.

Apart from the non-linearity of the cables, a long span cable-stayed bridge is very sensitive to both buffeting and flutter wind induced excitations, owing to its very light weight and slender nature. Although the above mentioned technique adopts a well defined continuous wind profile acting along the bridge deck and the vehicles, the wind loading effect is too simple and does not consider the wind induced flutter effect. This assumption has been proven to be reasonable for normal box-girder or slab-on-girder bridges. However, when considering the case of a long span cable-stayed bridge, the wind induced excitation mechanisms can be significant and should not be ignored.

3. Non-linearity and wind induced excitations on cable-stayed bridges

3.1. Cable sag and stiffness of cables

Nonlinear performance of the cable stayed bridge generally depends on the behaviour of the cables, stiffening girders and pylons. Nonlinearity of the cable originates with an increase in the loading followed by a decrease in the cable sag, which produces an elongation of the cable and corresponding axial tension. The stiffness of the cable-stayed bridge depends largely upon the tensile stiffness of the stay cables. The displacement of the end of the free hanging cable under an axial load depends not only on the cross-sectional area and the modulus of elasticity of the cable but, to a certain extent, on the cable sag, as proved by Ernst [10]. Considering an inclined cable under uniformly distributed loading, as shown in Fig. 2, it can be proven that the modulus of elasticity due to sag can be re-written in the form:

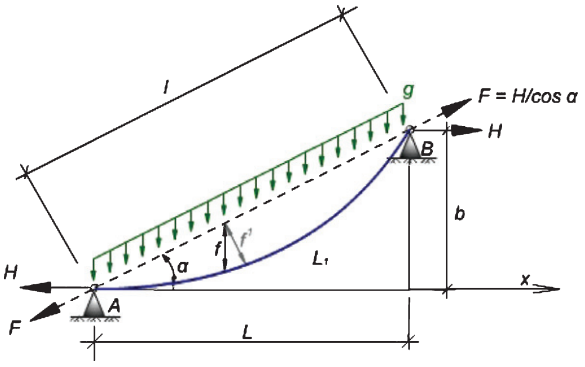

Fig. 2. Inclined cable under uniformly distributed loading.

$$E_f = \frac{12F^3}{A^3\gamma^2L^2} = \frac{12\sigma^3}{(\gamma L)^2} \tag{6}$$

Therefore,

$$E_i = \frac{E_e}{1 + \left[\frac{(\gamma L)^2}{12\sigma^3}\right] E_e} \tag{7}$$

where

E_i = Young's modulus of the cable having sag
E_e = Young's modulus of the straight cable
γ = Specific weight of the cable
L = horizontal length of the cable
σ = tensile stress in the cable.

For a straight locked-coil steel wire rope with Young's modulus of $1.52 \times 10^{10}\,\mathrm{kg/m^2}$, the approximate value of the specific weight is given by:

$$\gamma = \frac{g}{A} = 7584.3\,\mathrm{kg/m^3} \tag{8}$$

Equation 7 indicates that the ideal stiffness of a cable with sag depends on the actual length of the cable and the stress level of such cable. This essentially means that an iterative process is required to determine the exact effect of the cable sag.

3.2. Nonlinearity due to large displacement

The traditional finite element method and the stiffness method are based on small-deformation theory. In a cable-stayed bridge, the relatively large deformation of the superstructure under loading affects the value of the stresses in the structure. Therefore, the principle of superposition may be applied only with certain limitations. The problem of large deformation in cable-stayed bridges can be handled by the deformation theory or the so-called second order theory by taking into account the effect of the deflections of the structure in calculation the stresses and forces. When the equilibrium conditions are formulated for the geometry of the deformed structure, they are no longer linear. The internal forces of the bridge are not directly proportional, but grow at a faster rate than the external loading. Due to the deformations of the structure, there are additional stresses, which are not proportional to the additional loads. These stresses may be determined by the method of successive approximation. At the first stage, the stresses are calculated considering the initial geometry of the structure and applying the principles of linear analysis. The deformations obtained are further used to determine the modified geometry of the structure. At the second stage, linear analysis is again applied for the structure with modified geometry. This method is repeated until the deformations remain constant from one stage to the next. Two to five iterations are generally sufficient.

3.3. Implementation of geometrical non-linearity and cable sag in stability analysis

The ideal Young's modulus of the cables at a particular time can be determined from Eq. 7 and the internal force redistribution effect, due to the large deformation, can be determined using the successive approximation technique.

From Eq. 7, the stiffness of a cable varies with the tensile stress in the cable. On the other hand, the tensile force in a particular cable-stay inside a multi-cable system is a function of its stiffness. It is quite obvious that the actual cable force at a particular time instant has to be determined using an iterative approach. Moreover, as discussed previously, the successive approximation technique adopted to handle the non-linearity caused by large deformation is another application of the iterative approach. For an undeformed bridge with an initial stiffness matrix $[K_1]$, subjected to a static loading $\{F_1\}$, the following static equation applies:

$$[K_1]\{D_1\} = \{F_1\} \tag{9}$$

The initial deformation of the bridge $\{D\}$, can be evaluated from Eq. 9 with a given stiffness matrix and load vector. However, the deformation changes the geometry of the structure, as well as the length of all structural members. In addition, the ideal Young's modulus of the cables changes due to the internal redistribution of forces. These effects modify the stiffness matrix of the structure, and so Eq. 9 and the whole process is repeated until the redistribution of internal forces is minimal. When this iteration approach is applied to the direct integration process in the time domain, it follows that the iteration process should be applied to each time step.

Figure 3 demonstrates the simulation procedure within successive time steps for the vehicle performance simulation program for box-girder bridges. In each time step, displacement and position information is extracted from the previous time step without considering the nonlinearity of the cables and the large deformation. To make the vehicle performance simulation and the vehicle stability analysis applicable for long span cable-stayed bridges, an iterative process is inserted into the program between each time step and the overall procedure becomes that described in Fig. 4. In each time step, the initial values of displacements, stresses and forces are obtained from the direct integra-

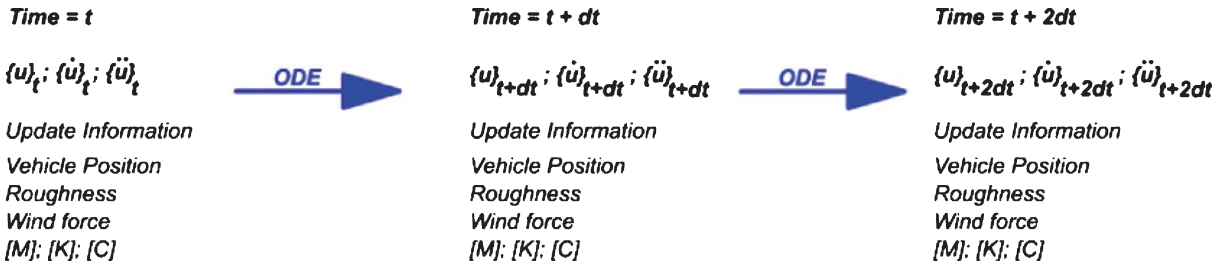

Fig. 3. Simulation processes without considering non-linear effects.

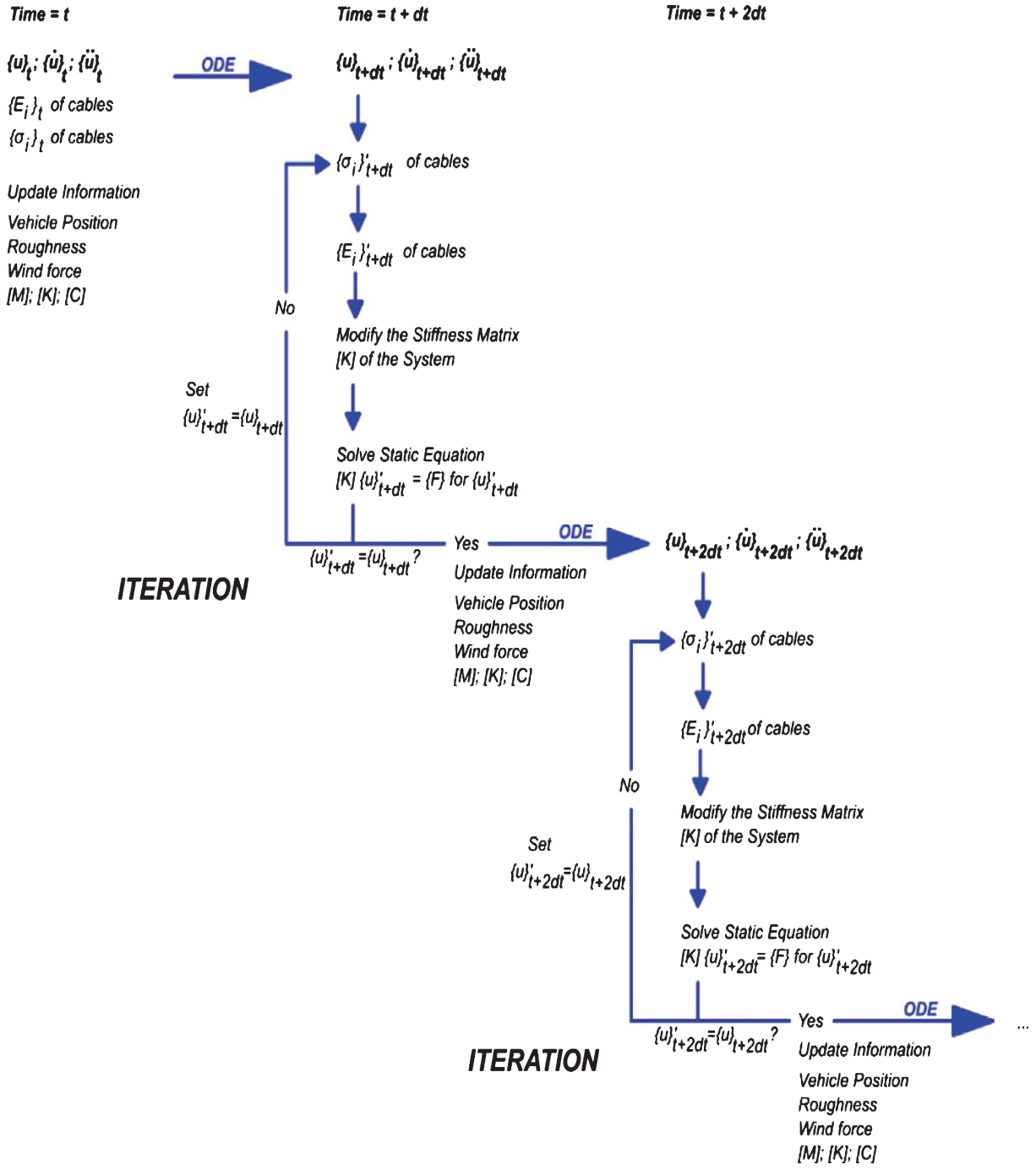

Fig. 4. Simulation process considering non-linear effects.

tion of the equations of motion of the coupled system in the previous step. These displacements and cable forces are then adopted to measure the change in sag in the cables and the change in the member's stiffness in the system, due to the large displacement. Based on the cable sag and the large displacement theory, the initial stiffness matrix is modified via Eq. 7 and the concept of successive approximations. By solving the static equation (Eq. 9) with the modified stiffness matrix, a new set of redistributed internal forces can be obtained. With

a different set of forces, the whole process is iterated until the internal forces remain at a constant value, or the variation falls to within an insignificant value. The iterative process determines the actual displacement profile and all the internal forces of the bridge subjected to the non-linear effects. The coupled system is then re-constructed, by locating the new position of the vehicles, the roughness at the contact point and the updated loading condition, before it is integrated in the next time step.

The procedure shown in Fig. 4 is very direct and is considered the simplest way to implement the non-linear effect in the vehicle stability analysis. Undoubtedly, a more reliable and accurate result can be achieved by undergoing an iterative process in each time step to evaluate the non-linear effect. However, this approach increases the simulation time dramatically. From the experience of the authors, up to 7–10 times the original simulation time is required to fully evaluate the non-linear effects in the simulation. To allow a higher efficiency, without ignoring the non-linear effect of cable sags and excessive deformation, the authors took advantage of an extremely small step size in the simulation process and proposed a Partial Iterative Procedure (PIP), as shown in Fig. 5. The direct integration in the time domain for the vehicle-wind-long span bridge system requires a relatively small step size, which is usually of the order of 10^{-4} of a second. Indeed, the step size is so small that it is possible to have part of the iterative process performed in one step and to continue the iterative process in the next time step. In Fig. 5, the static equation is solved once in a particular time step and the resulting displacements are adopted for the direct integration in the next time step. The whole process is continued in such a way that the direct integration and the iteration for non-linear effects is performed in parallel, in the time domain. The effectiveness and the efficiency of the proposed method will be demonstrated in the numerical example in the later section.

3.4. Wind induced effect on cable-stayed bridges

The wind velocity field adopted in structural analysis is usually reduced to some one-dimensional, multivariate stochastic processes and it is assumed that the wind induced effects between different dimensions are insignificant. However, this assumption might not be true when the wind effects on cable-stayed bridges are considered. For a flexible structure with a very high slenderness ratio, the cross-wind response becomes significant, as noted by Simiu and Scanlan [18]. These wind induced responses can cause very serious dynamic problems to the structure. Wind-induced vibrations in long span cable-stayed bridges can be classified into four types Troitsky [20], flutter; galloping; buffering

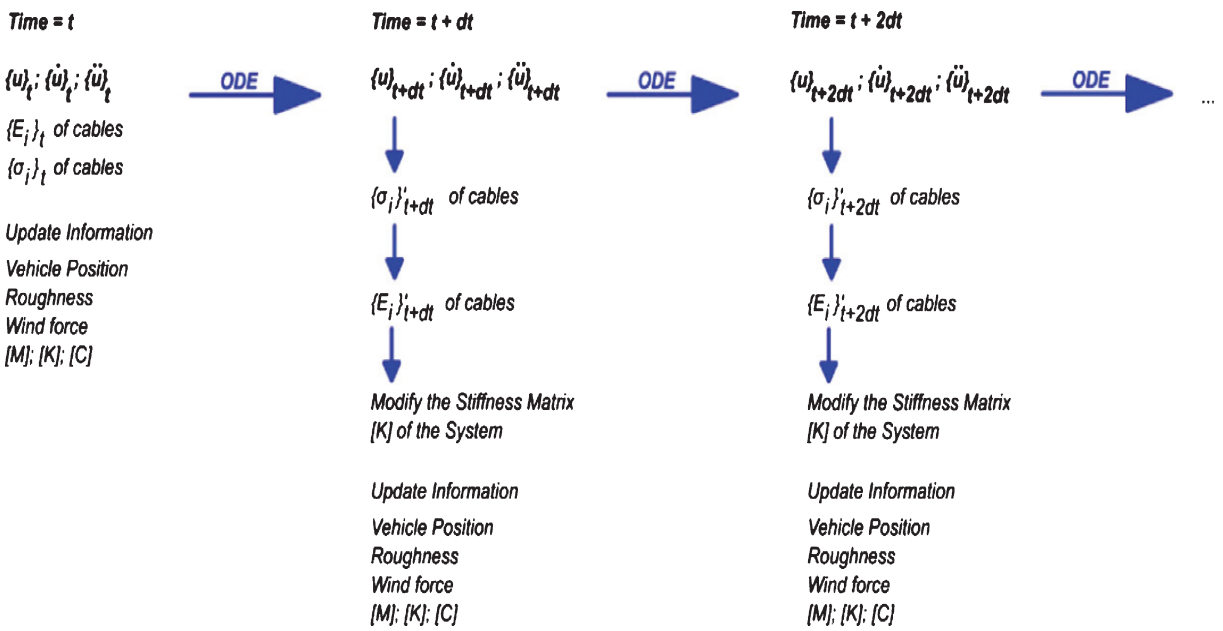

Fig. 5. Simplified parallel simulation process (PIT).

and vortex-induced vibrations. Among the above wind-induced vibration mechanisms, buffeting and flutter vibrations are considered the most critical in cable-stayed bridges subjected to wind loading under normal operational limits. When a slender bridge structure is subjected to a wind load of a certain critical wind velocity, instead of dissipating energy, the aerodynamic forces start to feed energy into the oscillating bridge structural system, resulting in the bridge vibrating in a divergent, destructive manner. According to Scanlan and Tomko [16], the classical flutter or binary flutter is driven by the stiffness of the air flow. For bridges, it is most likely to occur in cable-supported bridges with a streamlined flat deck cross-section.

Unlike the wind induced effect on relatively stiffer box-girder bridges, self-excited forces on cable-stayed bridges can be significant. It is suggested that galloping and some other self-excitation mechanisms, like lock-on excitation and vortex shedding, can be found in cables under rain-wind or snow-wind situations. These excitations on the cables do affect the vibration characteristics of the bridge, but galloping and vortex shedding usually require relatively high reduced velocity or under rain-wind situations. Besides, vortex shedding will only affect a few cables at a time due to the difference in cable length and the corresponding resonances. In view of the focus of this study, it is appropriate to ignore the self-excitation effect on the cables when studying the vehicle performance under operating wind velocities. On the other hand, the induced self-excitation effect on the bridge deck, such as buffeting and flutter, are considered the major wind induced excitation mechanisms for long span bridges, and have to be considered in the study.

3.5. Buffeting forces

The buffeting turbulence effects are described through the buffeting load component. The most simple load model is the quasi-steady one, in which the action of turbulence on each section is assumed to be independent of the natural frequency of the section and also the action on the contiguous sections. According to Simiu and Scanlan [18], if only vertical turbulence is taken into account, the buffeting lift and moment can be expressed by:

$$F_L(t) = qB\left[\frac{dC_L}{d\alpha} + C_D\right]\frac{w}{U} \tag{10}$$

$$M_a(t) = qB^2\frac{dC_M}{d\alpha}\frac{w}{U} \tag{11}$$

where q equals to $0.5\rho U^2$, with ρ is defined as the density of air and U is the mean wind speed. B is the width of the bridge deck, C_L and C_M are the aerodynamic coefficients defined as functions of the angle of attack (α). w is the vertical harmonic disturbances.

If frequency dependence is taken into account, the buffeting lift and moment can be corrected by aerodynamic admittance functions $\chi_{ij}(k)$, where the subscripts i and j identify the aerodynamic load component and the turbulence component, respectively. In this case, the subscript j can be omitted as there is only one turbulent component, the vertical turbulence w. Therefore, the buffeting force and moment can be expressed as:

$$F_L(t) = qB\left[\frac{dC_L}{d\alpha} + C_D\right]\frac{w}{U} \times \chi_L \tag{12}$$

$$M_a(t) = qB^2\frac{dC_M}{d\alpha}\frac{w}{U} \times \chi_M \tag{13}$$

with admittance functions $\chi_L(k)$ and $\chi_M(k)$.

Admittance functions are expressed as functions of $k = K/2$, where K is the reduced frequency. For bridge structures, the admittance functions can be measured in wind tunnel tests. When wind tunnel testing is not available, a reference admittance function for a thin airfoil, also known as the Sear's function, can be adopted, according to Fung [11].

3.6. Flutter forces

The governing equation of motion of the bridge subjected to turbulent wind loads can be expressed in terms of the generalized modal coordinates q as:

$$[M]\ddot{q} + [C]\dot{q} + [K]q = Q \tag{14}$$

where $[M]$ is the overall mass matrix of the vehicle-bridge system and it is a function of the position of the vehicles. $[C]$ and $[K]$ represent the overall damping matrix and the overall stiffness matrix of the corresponding system respectively. Q is the external load vector composed of the wind loading acting on the bridge and the vehicles, the equivalent buffeting force and also the equivalent fluttering force.

Self-excited forces are commonly modelled by means of frequency-dependent parameters (flutter derivatives H_p^* and A_p^*, with $p = 1, 2, 3, 4$), obtained experimentally through wind tunnel testing. The orig-

inal formulation is due to Scanlan in 1971, for two-dimensional bridge deck sections:

$$F_L(t) = qB\left[KH_1^*(K)\frac{\dot{z}(t)}{U} + KH_2^*(K)\frac{B\dot{\alpha}(t)}{U} + K^2H_3^*(K)\alpha(t) + K^2H_4^*(K)\frac{\dot{z}(t)}{U}\right] \quad (15)$$

$$M_a(t) = qB^2\left[KA_1^*(K)\frac{\dot{z}(t)}{U} + KA_2^*(K)\frac{B\dot{\alpha}(t)}{U} + K^2A_3^*(K)\alpha(t) + K^2A_4^*(K)\frac{z(t)}{U}\right] \quad (16)$$

where t is the time, U is the average wind velocity acting on the bridge deck and B is the width of the bridge deck; $z(t)$ and $\alpha(t)$ are the vertical and rotational displacement profiles respectively.

Flutter derivatives offer the greatest advantage of being extracted through a quite consolidated approach, but they are not well suited for time-domain simulations, as they are expressed as functions of reduced velocity U_{red}, with $U_{red} = U/fB = 2\pi/K$, where K is the reduced frequency.

An alternative approach, offered by the pure time-domain formulation via indicial functions proposed by Scanlan and Tomko [16] and further discussed by Borri et al. [3], is adopted here. Costa and Borri [9] proposed a specific formulation for a two-dimensional bridge deck section, in which:

$$F_L(s) = qB\frac{dC_L}{d\alpha}\left[\phi_{L\alpha}(0)\alpha(s) + \phi_{Lz}(0)z'(s) + \int_0^s \phi'_{L\alpha}(s-\tau)\alpha(\tau)d\tau + \int_0^s \phi'_{Lz}(s-\tau)z'(\tau)d\tau\right] \quad (17)$$

$$M_a(s) = qB^2\frac{dC_M}{d\alpha}\left[\phi_{M\alpha}(0)\alpha(s) + \phi_{Mz}(0)z'(s) + \int_0^s \phi'_{M\alpha}(s-\tau)\alpha(\tau)d\tau + \int_0^s \phi'_{Mz}(s-\tau)z'(\tau)d\tau\right] \quad (18)$$

where s is dimensionless time defined as $s = Ut/b$ and the prime denotes differentiation with respect to s.

Indicial functions are defined as the superposition of m exponential groups:

$$\phi_{il}(s) = 1 - \sum_{k=1}^{m}\alpha_{ilk}e^{-b_{ilk}s} \quad (19)$$

Subscripts i and l identify the load component (L = lift; M = moment) and the motion component that experiences a unit step change respectively. Each indicial function describes the non-stationary evolution in time of the load due to a unit step change in the angle of attack. In this model, torsional displacement ($l = \alpha$) and vertical velocity ($l = z$) contribute to define the angle of attack. Therefore, two indicial functions result for each force component.

The identification of the indicial function coefficients is performed by comparison of the load model equations in the time domain (Eqs 16–17), with the equations in the reduced frequency domain (Eqs 14–15). The relationships between these equations are stated in Costa and Borri [9]. Self-excited forces are calculated via convolution, accounting for motion histories expressed as a series of infinitesimal step-wise increments. It is noted that the "airfoil convention" is adopted in Costa's load representation, where the lift force is positive upwards and the aerodynamic moment is positive clockwise. Attention must be paid to the different conventions concerning lift in Scanlan's formulation, in which lift is usually positive downwards

3.7. Implementation of wind induced effect on vehicle simulation package

At any particular time t the wind velocity at a node (i) on the bridge deck can be determined from the wind velocity time-history at that node. The corresponding the buffeting and flutter effects can be calculated via Eqs 12–13 and Eqs 17–18, respectively. These wind forces are considered as extra external forces acting on the structure, and are functions of time and motion of the structure. In the simulation process, the extra external forces at any time instant can be determined from the motion of the system in the previous time-step and are added into the system (Eq. 5) as an external force vector.

4. Vehicle stability and reliability analysis

The simulation module precisely descripts the vibration of vehicle throughout the journey. The performance assessment module, on the other hand, assesses the safety of the vehicle at any time instant by re-defining

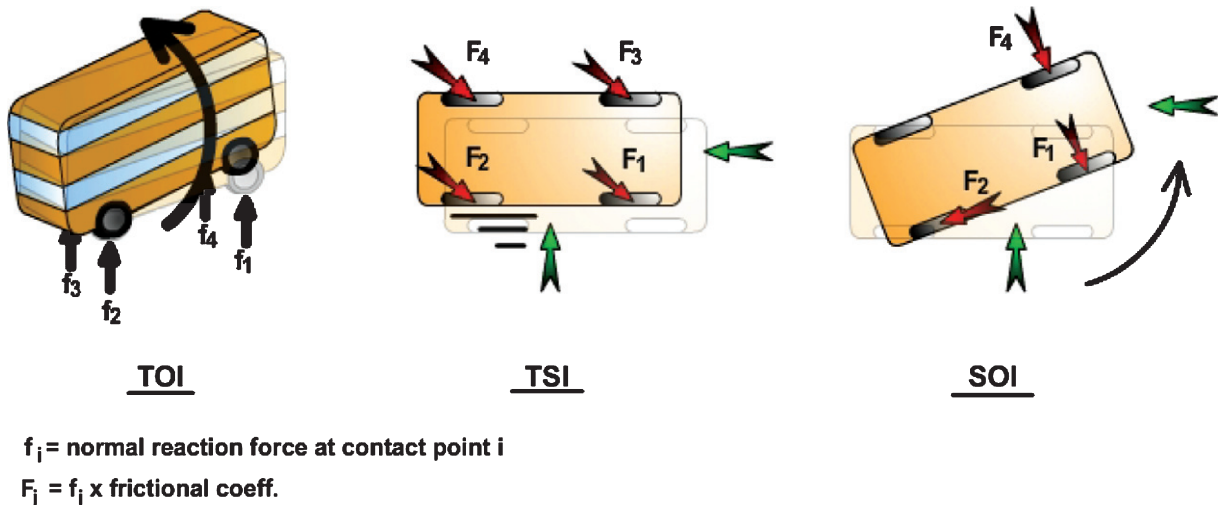

Fig. 6. Vehicle instability situations.

the vehicle instability criteria as shown in Fig. 6. The overturning moment is resisted by the couple due to the self-weight and the normal reaction forces on the wheels, while the frictional force available depends on the frictional coefficient and the normal reaction forces on the wheels. The normal reaction forces on the tyres can be evaluated by re-solving the interaction forces at the contact point used for the vehicle system. The frictional coefficient, however, varies considerably with the road condition. According to information given by the Niigata Experimental Laboratory of the Public Works Research Institute in Japan, the frictional coefficient is in the range 0.8–0.9 for dry conditions; 0.7 for wet conditions and 0.4–0.5 for conditions with a thick water film on the road. By considering the free-body diagram of the vehicle, a set of vehicle instability constraint equations can be constructed.

The motion of the vehicles are calculated and checked against these instability constraints at each time step to evaluate the stability condition of the vehicle during the drive. The overall stability analysis procedure is summarised in Fig. 8. In addition, the time required for the reliability analysis can be significantly reduced by using the continuous simulation procedure proposed by Cheung and Chan [8]. The overall reliability analysis technique has been proven to be effective for box-girder bridges.

5. Numerical example – Kap Shui Mun Bridge

The Kap Shui Mun Bridge in Hong Kong is the longest cable-stayed bridge in the world that transports both road and railway traffic. It has a main span of 430 m and an overall length of 750 m. It spans the main marine channel, Kap Shui Mun, between Ma Wan and Lantau and provides a vertical clearance of 47 m above sea level.

5.1. Bridge model

To demonstrate the application of the vehicle instability analysis on cable-stayed bridges, a finite element bridge model is constructed with the bridge deck being modelled as 3D beam elements connected by rigid "dummy arms" and the towers are modelled as frame elements, as shown in Fig. 9. The stay cables are modelled as 3D truss elements with an effective Young's modulus determined by Eq. 7. Figure 10 shows the material properties of the cables. It is noted that the initial cable forces are modelled as temperature loading and the detail of the initial cable temperature loads can be found in Chan [6]. The overall consistent mass matrix and the overall stiffness matrix are constructed using traditional finite element techniques. The stiffness matrix is constructed directly using the conventional stiffness method. To verify the accuracy of the stiffness matrix, some static loading cases have been studied. A force vector is constructed for each loading case and the displacement of the structure subjected to these static forces can be evaluated by solving the classical static system:

$$[K][D] = [F] \tag{20}$$

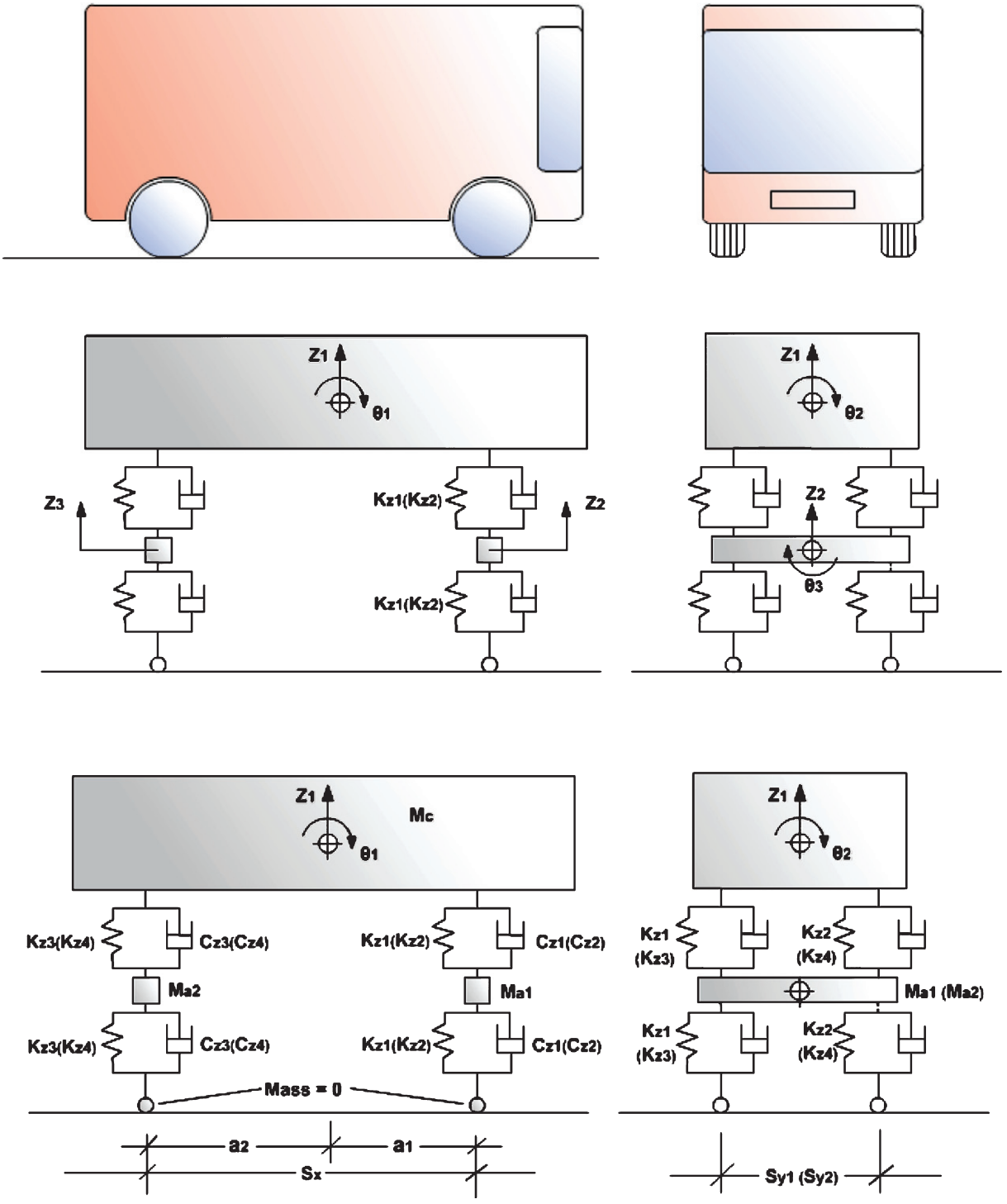

Fig. 7. Vehicle model.

where [K] is the stiffness matrix of the structure; [D] is the displacement vector and [F] is the force vector. The displacements are compared with the result obtained from SAP2000, which has been calibrated and verified by Yang [23]. The displacement results are identical to the result obtained from the SAP2000 model for all

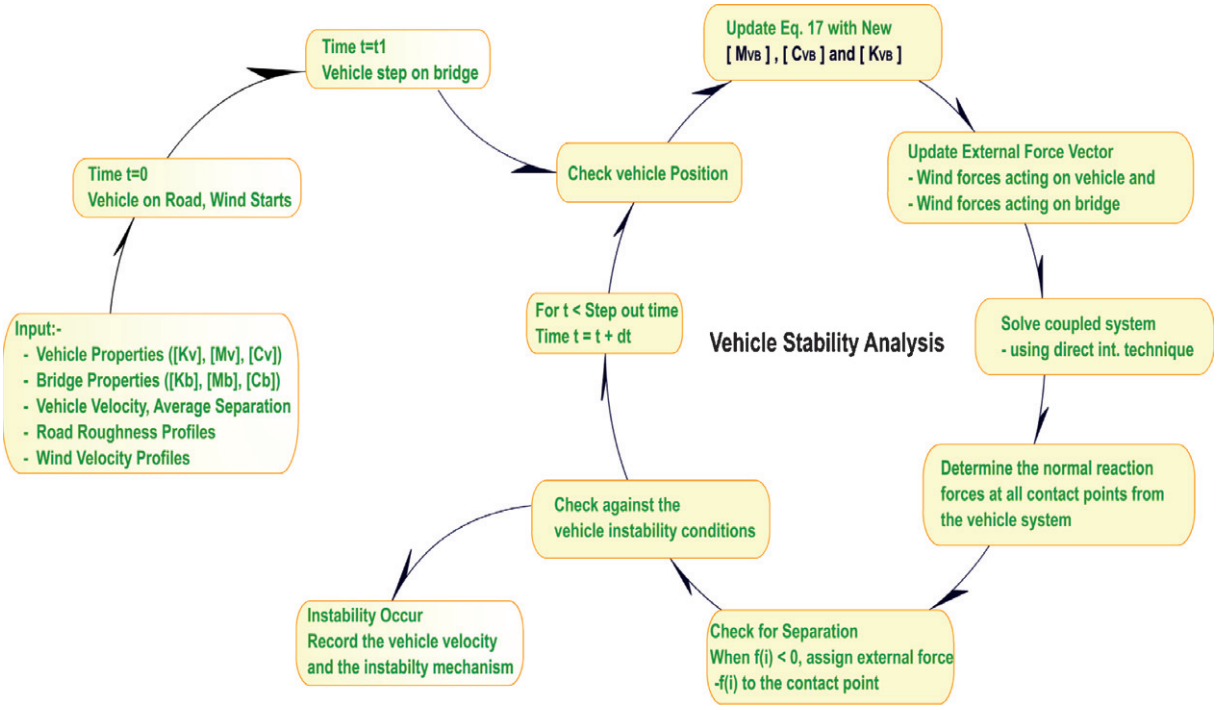

Fig. 8. Overall procedures for vehicle stability analysis.

the static cases, indicating that the stiffness matrix is correctly constructed.

5.2. Vehicle models

A typical high-sided vehicle, the double decker bus, and a small very small private car, the "Kai" car, were examined in this study. The high-sided vehicle adopted in this example is the "Enviro Trident" double-decker bus which has been operating in HK since 2003, and has dimensions of $12\,\text{m} \times 2.55\,\text{m} \times 4.3\,\text{m}$. Figure 11 shows the photo and some general specifications of the vehicle. The gross mass of the empty vehicle is 23500 kg. A 7-degree-of-freedom, 2-axle four-wheel vehicle model, proposed by Cheung and Chan [8] as illustrated in Fig. 7, was created with the following parameters:

For the double-decker bus,

$m_c = 23500\,\text{kg}$;	$m_{a1} = 1800\,\text{kg}$;	$m_{a2} = 4700\,\text{kg}$;
$I_c = 380000\,\text{kg m}^2$;	$I_t = 42000\,\text{kg m}^2$;	$I_{a1} = 1100\,\text{kg m}^2$;
$I_{a2} = 1600\,\text{kg m}^2$;	$S_x = 9.2\,\text{m}$;	$S_{y1} = 2.4\,\text{m}$;
$S_{y2} = 2.4\,\text{m}$;	$a_1 = 0.55$;	$a_2 = 0.45$;
$l = 12\,\text{m}$;	$b = 2.55\,\text{m}$;	$h = 4.3\,\text{m}$;

For the Kai car,

$m_c = 800\,\text{kg}$;	$m_{a1} = 65\,\text{kg}$;	$m_{a2} = 90\,\text{kg}$;
$I_c = 3600\,\text{kg m}^2$;	$I_t = 2400\,\text{kg m}^2$;	$I_{a1} = 200\,\text{kg m}^2$;
$I_{a2} = 250\,\text{kg m}^2$;	$S_x = 3.1\,\text{m}$;	$S_{y1} = 1.5\,\text{m}$;
$S_{y2} = 0.8\,\text{m}$;	$a_1 = 0.6$;	$a_2 = 0.4$;
$l = 4.08\,\text{m}$;	$b = 1.635\,\text{m}$;	$h = 1.485\,\text{m}$;

5.3. Identification of flutter derivatives

The identification of the lift and moment flutter derivatives can be obtained from free vibration tests in smooth flow within a boundary layer wind tunnel. The flutter derivatives are then derived using a unifying least square technique proposed by Gu et al. [12]. In this numerical example, the flutter derivatives information is not available and therefore, the flutter derivatives of a similar cable-stayed bridge obtained from Gu are assumed for simplicity. The identified moment flutter derivatives are plotted against the reduced velocities in Fig. 12 and the identified lift flutter derivatives are plotted against the reduced velocities in Fig. 13. The reduced velocities are obtained by normalizing the velocities with respect to natural vertical and torsional

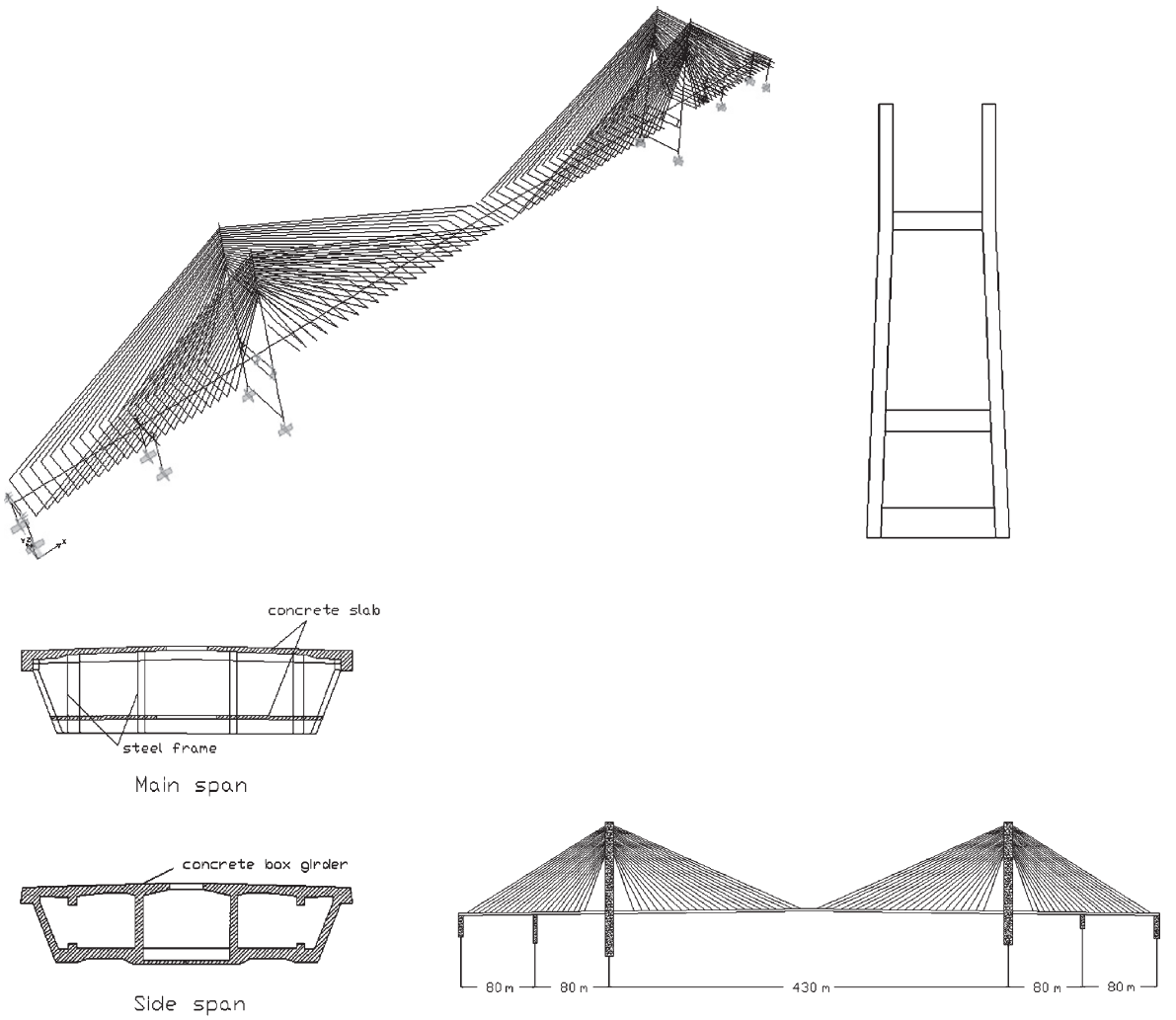

Carriage: 6 lanes of roadways on upper deck, 2 lanes of MTR rails on the lower deck,
Total length: 750 m; Longest span: 430 m; Deck width: 32.5 m; Number of cables: $8 \times 22 = 176$;
Concrete strength: Grade 50/20.

Fig. 9. 3D frame model of Kap Shui Mun Bridge.

frequencies. Following the indicial functions procedure discussed earlier in this paper, the load model equations in the reduced frequency domain, Eqs 18–19, can be expressed in terms of the flutter derivatives given in Figs 12 and 13. By comparing the above equations with the load model of the equations in the time domain, the indicial function coefficients can be determined. The indicial function coefficients are summarized in Table 1. Using the indicial coefficients, the aerodynamic derivatives are estimated, giving $dC_L/d\alpha$ and $dC_M/d\alpha$ values of 4.60 and 1.45 respectively. The flutter and buffeting forces are expressed in terms of the displacements of the bridge deck, the velocities of the bridge deck and the wind velocities at the particular time instant. These forces are treated as extra external forces in addition to the wind loading caused by the wind velocity profiles.

5.4. *Wind velocity profiles and the road roughness profiles*

The wind velocity profiles and the road roughness profiles for the cable-stayed bridge are generated using

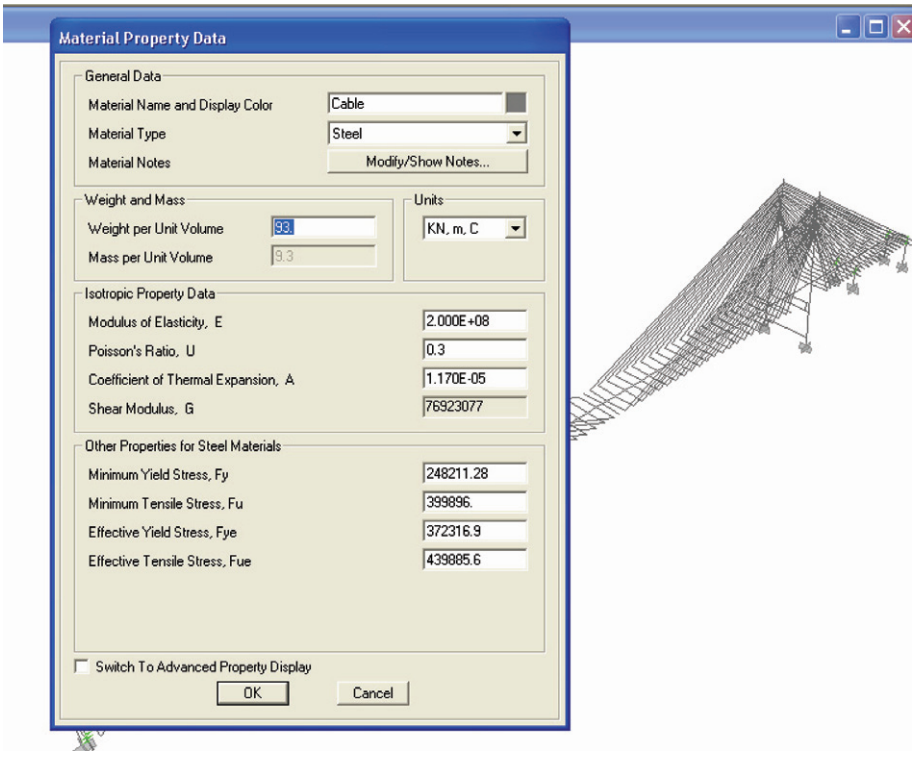

Fig. 10. Material properties for cables.

WEIGHT DATA

Model	12.0m
Front Axle plated weight	7,500 kgs
Drive Axle plated weight	9,500 kgs
Tag Axle plated weight	6,500 kgs
Gross plated weight	23,500 kgs

DIMENSIONS

Model	12.0 m Complete Vehicle	Chassis Only
Overall length	11,999 mm	11,809 mm
Wheelbase	5,700 mm+1,500 mm drive axle	
Overall width	2,550 mm	2,550 mm
Overall height	4,267 mm	-
Front overhang	2,414 mm	2,239 mm
Rear overhang	2,385 mm	2,370 mm

Fig. 11. Specification of a double-decker bus.

an identical approach as for a box-girder bridge introduced by Chan [6]. For the wind velocity profiles, 50 uniformly distributed profiles are generated along the bridge deck. The total length of the bridge is 750 m, which indicates that the distance between successive wind velocity profiles is 15 m. With an upper cut-

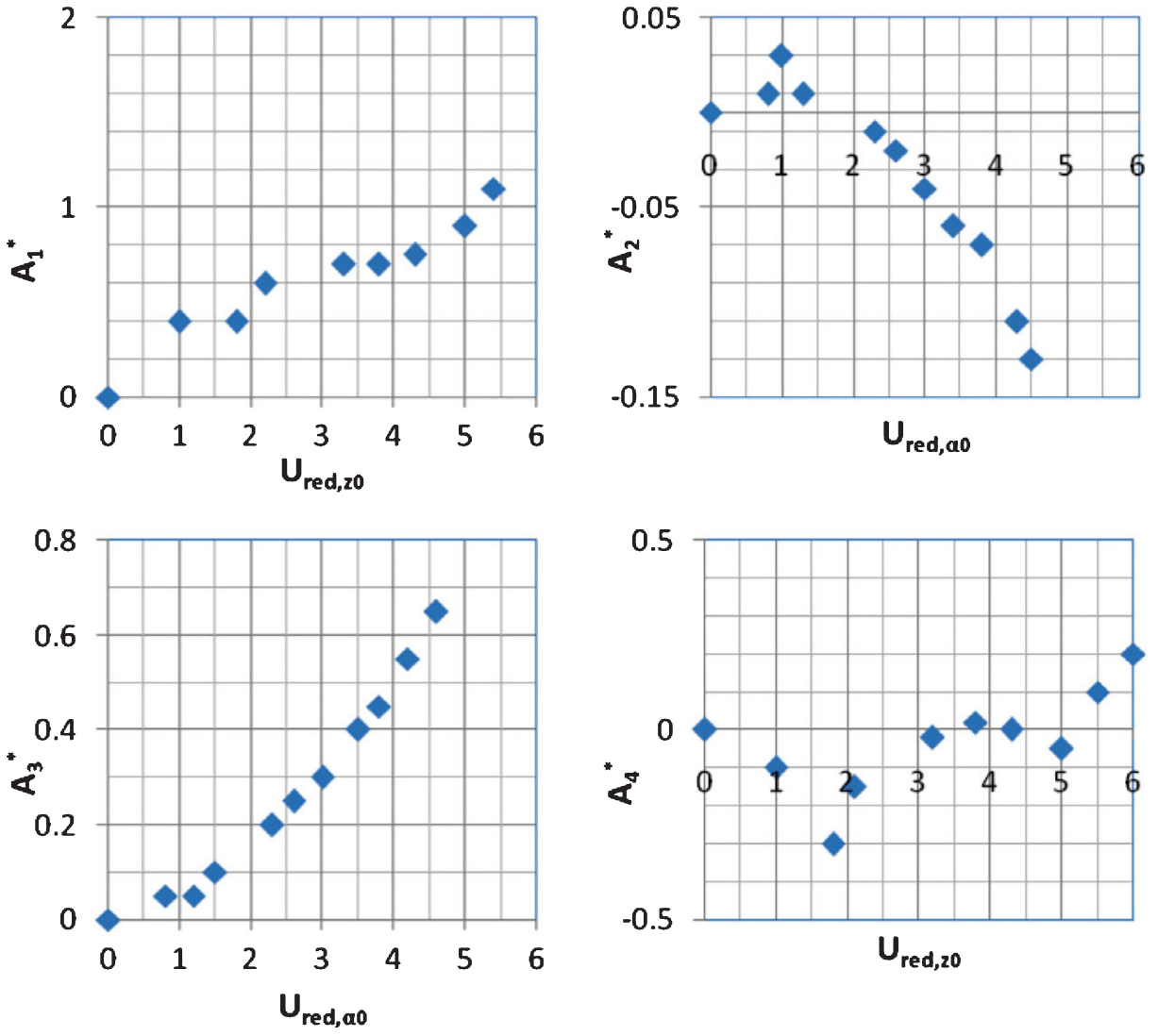

Fig. 12. Moment flutter derivatives (A_1^* to A_4^*) using ULS method.

off frequency of 4π rad/s, wind data are generated using the spectral representation method developed by Shinozuka and Deodatis [17] with the following parameters:

Data adopted in wind velocity profile simulation:

- Bridge span: $L = 750$ m
- Height of deck above ground: $z = 47$ m
- Ground roughness: $z_0 = 0.03$ m
- Average horizontal wind velocity: $U(z) = 10$ m/s to 60 m/s
- Upper cut-off frequency: 4π rad/s
- Dividing number of frequency: $N = 1{,}024$
- Target wind spectrum: Kaimal's spectrum for wind velocity profile

5.5. Analysis and results

5.5.1. Effectiveness of the proposed partial iterative procedure (PIP)

The non-linear behaviour of the cable-stayed bridge is considered by inserting an iterative procedure in each integration time step. In addition, an alternative partial iterative technique is proposed to handle the non-linear behaviour of the bridge, without dramatically lengthening the simulation time. In this example, three different approaches in handling the non-linear behaviour of the bridge are compared, and the accuracy and effectiveness of these approaches is studied. The first approach is the fully iterative approach, with a full

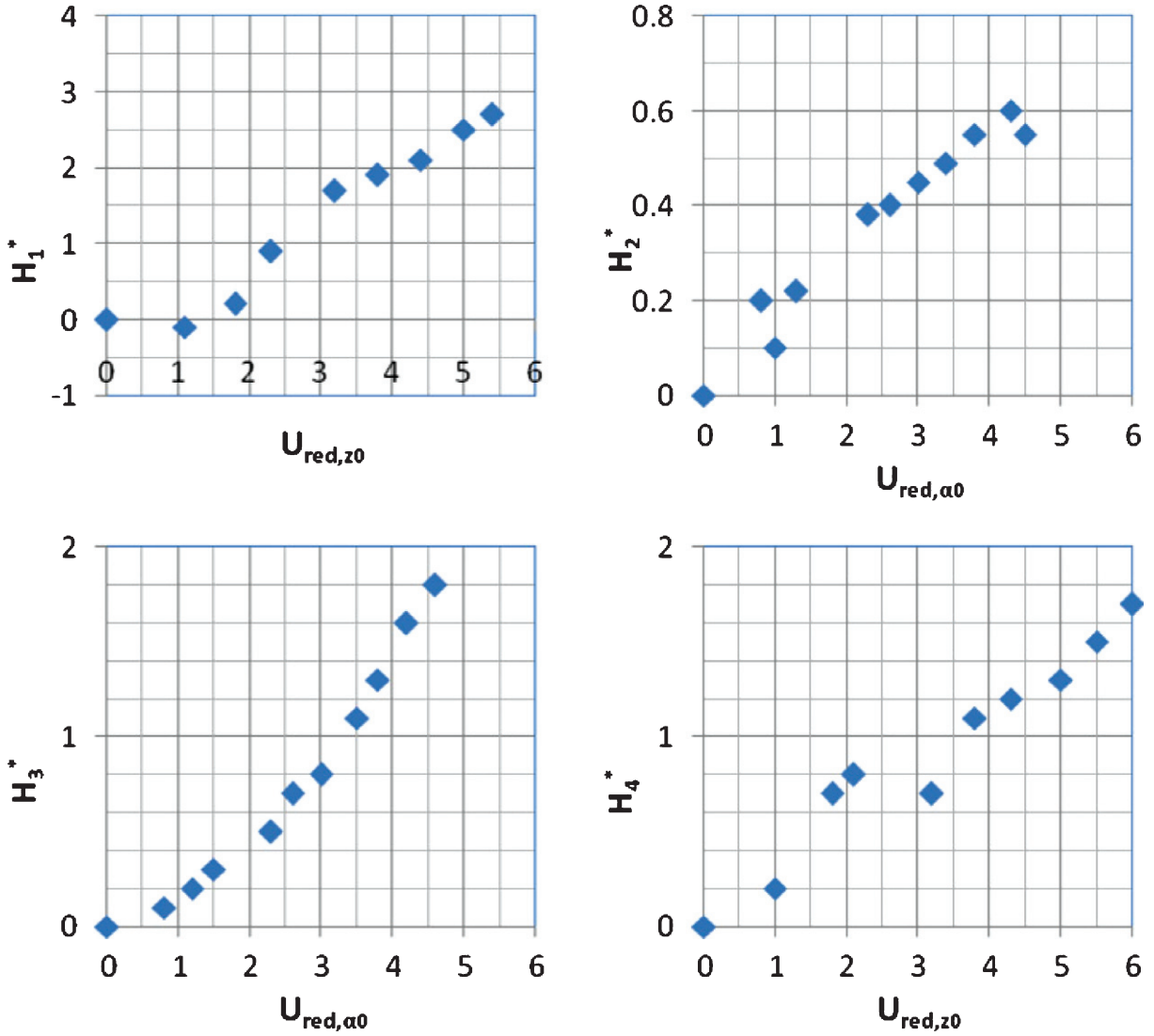

Fig. 13. Lift flutter derivatives (H_1^* to H_4^*) using ULS method.

Table 1
Assumed indicial function coefficients for the bridge

Indicial function	Φ_{Lz}	Φ_{Mz}	$\Phi_{L\alpha}$	$\Phi_{M\alpha}$
a	0.932	–0.228	–4.815	0.611
b	1.125	4.633	0.711	0.092

iteration inserted between the time steps. The general procedure is described in Fig. 4. The second approach is the proposed partial iterative approach using the PIT as introduced in Fig. 5. Finally, linear analysis, without considering the non-linear effect, is adopted for control comparison.

A chain of 100 double-deckers are allowed to pass along the bridge subject to an average wind velocity of 30 m/s. The total simulation time for each of the three approaches is summarized in Table 2. It is demonstrated that the proposed approach is very effective, and only requires less than 1/5 of the total simulation time required when using the fully iterative approach. In terms of accuracy, the non-linear effects of cable sag and the excessive deformation will cause a redistribu-

Table 2
Simulation time for different approaches

Approach	Simulation time in VPSIM
Fully iterative approach	23.5 hrs
Parallel iterative technique	3.5 hrs
No iteration	2.5 hrs

tion of internal forces in the stay cables and within the deck, and the change in cable force in the longest cable stay connecting the east tower and the mid-span during the simulation is illustrated in Fig. 14. From the figure, when the cable force increases, both non-linear approaches give a higher tensile value when compared with the linear approach. This is a reasonable outcome, since the increase of the cable force increases causes the stiffness of the cable to increase, according to Eq. 7, and it tends to attain more force. On the other hand, it is suggested that the non-linear effects can be very significant in a cable-stayed bridge, demonstrated by the large difference in cable force between the linear and the non-linear approach. However, in the same figure, there is not much difference in cable force between the fully iterative approach and the proposed partial iterative approach using PIP, which suggests that the proposed approach can also correctly capture the non-linear behaviour of the bridge. It is suggested that the proposed approach using PIP can effectively and more efficiently capture the non-linear behaviour of a cable-stayed bridge.

5.6. Operational speed limit on bridges

To study to operational speed limit for a vehicle travelling on the Kap Shui Mun Bridge using the proposed continuous simulation procedure, continuous wind events, with mean wind velocities ranging from 10 m/s to 40 m/s, are generated and a chain of vehicles moving along the bridge is simulated. For each wind event, the maximum vehicle velocity that allows no instability for 500 vehicles is recorded. The maximum allowable vehicle velocities at different wind levels are plotted against average wind velocities in Fig. 15. For double-deckers travelling on Kap Shui Mun Bridge, as shown in Fig. 15(a), vehicle instability is governed by the overturning instability at high wind speeds (above 25 m/s) and sliding instability at moderate to low wind speeds. For the Kai car, as shown in Fig. 15(b), instability situations are governed by total sliding and side-slip overturning for all wind speeds within the serviceability range. The overall allowable speed limit for the Kap Shui Mun Bridge is demonstrated in Fig. 15(c), by combining the two extreme cases mentioned above. The simulation result demonstrated that each of the instability mechanisms can be the governing one, and vehicles with different dimensions may be subjected to different instability conditions in the same environment.

As a demonstration on how the vehicle-wind-bridge interaction affect the allowable vehicle speed limit, Fig. 16 shows the operational requirements for the Confederation Bridge in Canada, a typical modern box-girder bridge. When compared with the Confederation Bridge, instability conditions are identified at much lower wind/vehicle speeds. This phenomenon can be explained by the amplification of the coupling interaction forces in the coupled system. For the more flexible Kap Shui Mun Bridge subject to vehicle and wind loadings, the bridge together with the vehicles, displaces with larger amplitudes. The amplified vibration increases the interaction between the bridge and the vehicles. This more vigorous interaction results in a higher chance of adverse conditions in the random simulation process.

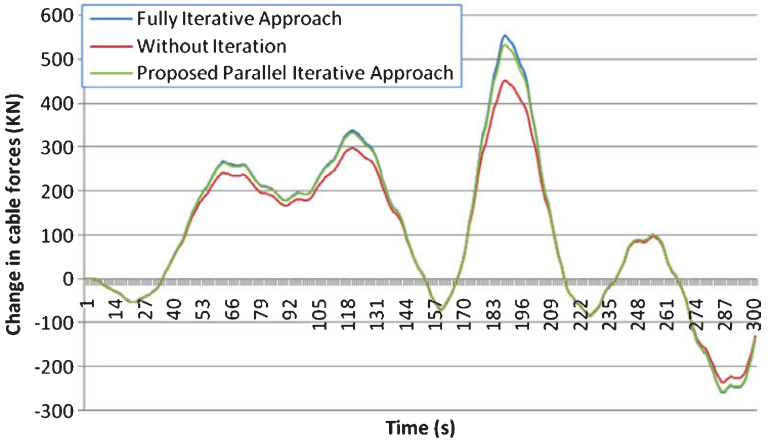

Fig. 14. Change in cable force using different approaches.

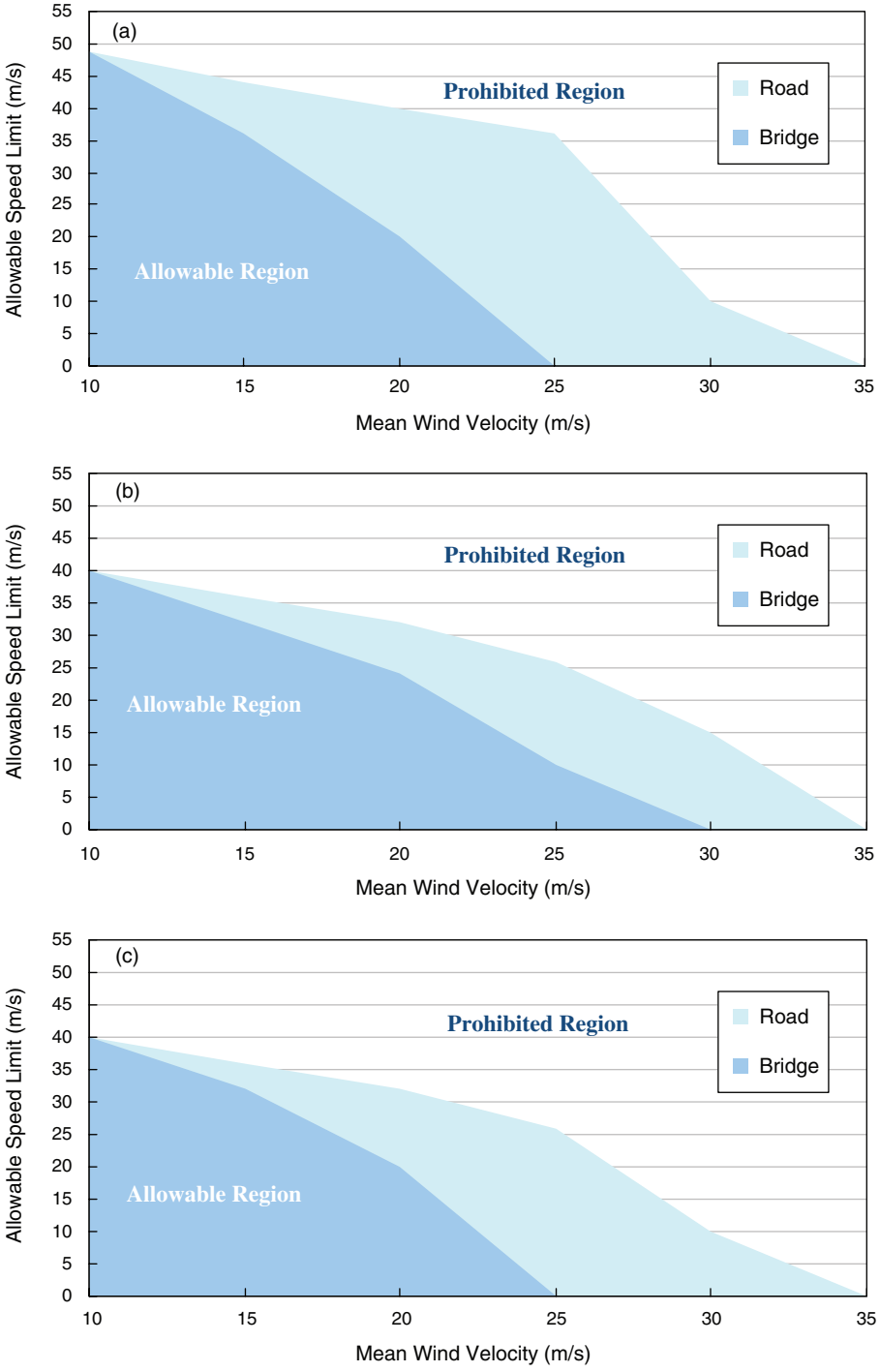

Fig. 15. Operational requirements for the Kap Shui Mun Bridge, (a) Double-Decker, (b) Kai-car, (c) Overall.

6. Conclusion

In view of the importance of maximizing the transportation capacity of cable-stayed bridges during windy period, this research provides a general and realistic approach to predict the appropriate permissible speed limit for vehicles travelling on bridges, without the need of extensive wind tunnel tests, which are time consum-

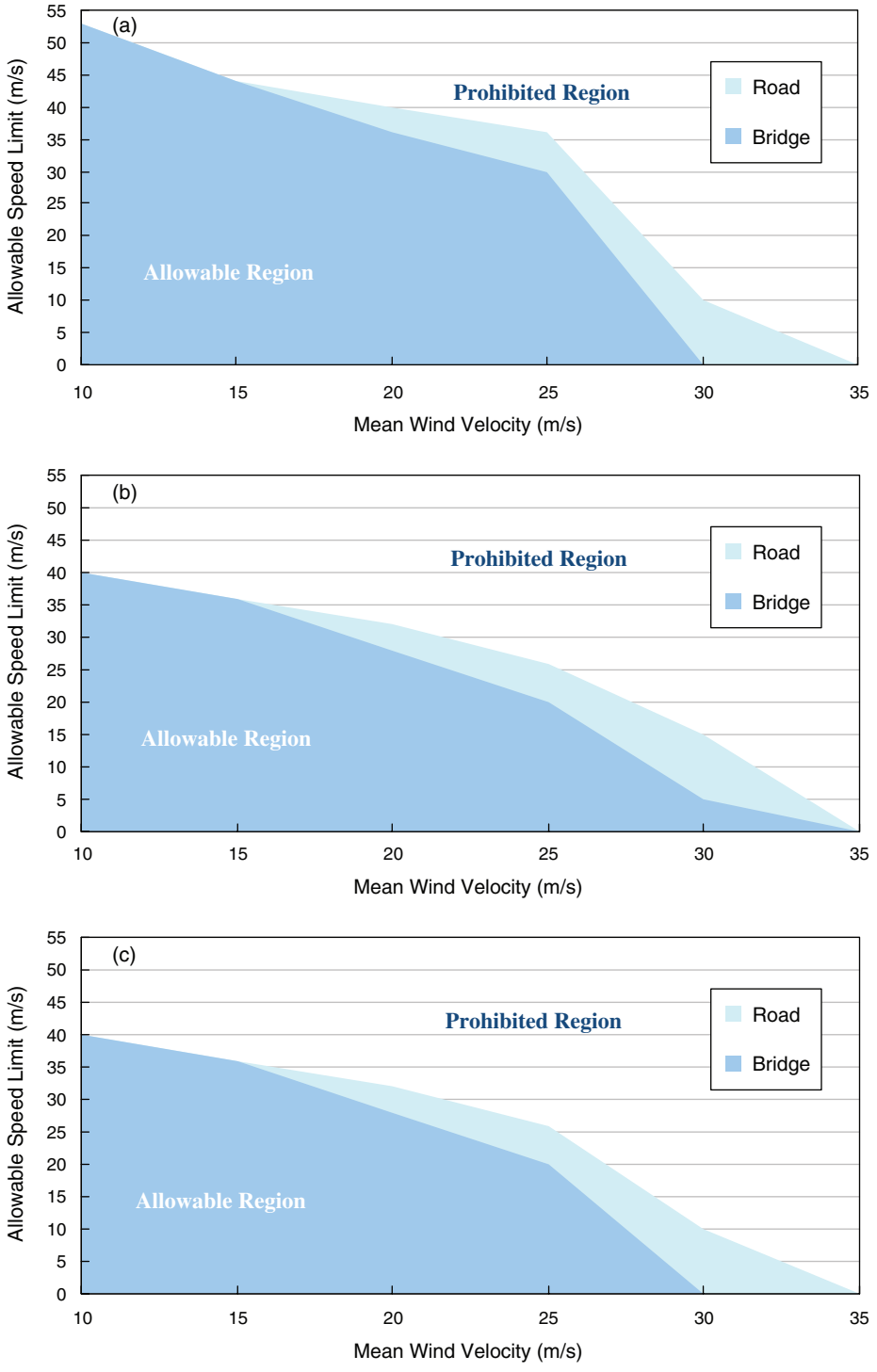

Fig. 16. Operational requirements for the Confederation Bridge, (a) Double-Decker, (b) Kai-car, (c) Overall.

ing and expensive. In handling the flexible cable-stayed structures, cable sag, moment redistribution due to large displacements and wind induced excitations are well considered in the simulation module. The PIP handles the non-linear effects, including the cable sag and the effect of large displacements. Besides, the flutter and

buffeting effects are taken into account by transforming this effect into equivalent flutter and buffering forces and moments acting on the coupled system. By incorporating the interaction model in the set of instability criteria, developed from the stepwise free-body diagram of the vehicle-bridge system, the stability of vehicles on bridges can be evaluated.

For high-sided vehicles, total overturning instability tends to be the governing instability condition when the mean wind velocity is extremely high, while total sliding instability and side-slip overturning govern the instability conditions under low to moderate wind velocities. It is also observed that the vehicle instability problem is highly coupled and is composed of many random factors, and vehicle instability does not necessarily occur at the mid-span with the highest wind velocity. This indicates that the operational requirements can only be estimated by a statistical analysis and the proposed method, together with the continuous simulation technique provides a possible solution.

Including Baker's findings [1, 2], many researchers showed that high-sided vehicles, such as double-deckers, can overturn on roads when subjected to strong wind conditions. It is generally believed that a high-sided vehicle is more prone to strong wind induced instability. For some modern bridges, wind tunnel tests are conducted to study the minimum wind speed that causes overturning of a stationary high-sided vehicle model on the bridge, and this value is adopted as the basis for setting up the operational requirement of the bridge. However, the simulation result in this study suggests that the allowable speed limit on bridge is not necessarily governed by high-sided vehicles. Although having a very strong resistance against overturning instability, even in very high wind speeds, light weight vehicles suffer significantly from total sliding and side-slip overturning, under relatively low wind velocities.

It is proposed that a two-phase allowable speed limit should be imposed on a bridge. When the wind speed is not too high, the allowable speed limit, which decreases proportionally to the wind speed, should be imposed to prevent sliding instability of light vehicles. In addition, the operation of double-deck buses must be stopped during very strong wind events to avoid overturning instability of such vehicles.

Besides, the simulation results also suggest that the vehicle-wind-bridge interactions are much stronger on cable-stayed bridges, when compared with the interactions on box-girder bridges. This strong interaction increases the probability of having an adverse stability situation when a vehicle is travelling on the bridge. This explains the phenomenon where a vehicle becomes unstable on cable-stayed bridges at a much lower wind speed than a vehicle on an off-bridge road.

The ultimate goal of this study is to provide an effective, yet accurate, estimation on the operational requirement of cable-stayed bridges, which is very useful for bridge managers and planners, in term of bridge management. However, other hazards must also be considered when setting up the operational requirements for a long span bridge, including debris and other flying objects on the bridge, driving behaviour and the driver's reaction in severe winds. Besides, studies demonstrated that driver's experience and reactions can stabilize the displacement performance of vehicles and prevent the occurrence of instability conditions. The effect of human behaviour, however, is not considered in this study as the authors believe that it is unfair to assume that drivers are experienced. The fact is that, inexperienced drivers might not be able to handle unexpected wind gusts and their reactions are difficult to predict. Therefore, more studies shall be conducted to estimate such stabilization effect caused by the driver's behaviour on the vehicle performance.

Acknowledgements

The authors wish to gratefully acknowledge the financial support of the Hong Kong Research Grant Council RGC No. 612207 for the project on Operational Requirements for Long Span Bridges under Strong Wind Conditions.

References

[1] C.J. Baker, A simplified analysis of various types of wind-induced vehicle accidents, *J Wind Eng Ind Aerodyn* **22** (1986), 69–85.

[2] C.J. Baker, Ground vehicles in high cross winds: The interaction of aerodynamic forces and the vehicle system, *Journal of Fluids and Structures* **5** (1991), 221–141.

[3] C. Borri, L. Salvatori and W. Zahlten, Finite-element time-domain simulations of bridge aeroelasticity, *Computat Fluid Solid Mech* **1** (2005), 103–107.

[4] C.S. Cai and S.R. Chen, Framework of vehicle-bridge-wind dynamic analysis, *J Wind Eng Ind Aerodyn* **92** (2004), 579–607.

[5] Y. Cao, H. Xiang and Y. Zhou, Simulation of stochastic wind velocity field on long-span bridges, *J Eng Mech ASCE* **1261**(1) (2000), 1–6.

[6] Y.B. Chan, Vehicle-Wind-Long Span Bridges interactions and its effect on speed limit and vehicle stability, PhD Thesis, 2008, HKUST, HK.

[7] S.R. Chen and C.S. Cai, Accident assessment of vehicles on long-span bridges in windy environments, *J Wind Eng Ind Aerodyn* **92**(12) (2004), 991–1024.
[8] M.M.S. Cheung and B.Y.B. Chan, Operational requirements for long span bridges under strong wind events, *Journal of Bridge Engineering, ASCE* **15**(2) (March/April 2010), 131–143.
[9] C. Costa and C. Borri, Application of indicial function in bridge deck aeroelasticity, *J Wind Eng Ind Aerodyn* **94** (2006), 859–881.
[10] J.H. Ernst, Der E-modul von Seilen unter Berücksichtigung des Durchhanges, *Der Bauingenieur* **40**(2) (1965), 52–55.
[11] Y.C. Fung, *An Introduction to the Theory of Aeroelasticity*, Dover Publication, Inc., Mineola, New York, 1996.
[12] M. Gu, R. Zhang and H. Xiang, Identification of flutter derivatives of bridge, *J Wind Eng Ind Aerodyn* **84** (2000), 151–162.
[13] W.H. Guo and Y.L. Xu, Safety analysis of moving road vehicles on a long bridge under crosswind, *Journal of Engineering Mechanics* **132**(4) (2006), 438–446.
[14] R.J. Jiang, F.T.K. Au and K.Y. Cheung, Identification of vehicles moving on continuous bridges with rough surface, *Journal of Sound and Vibration* **274** (2004), 1045–1063.
[15] C.H. Liu, Simulation of divers correlative stochastic processes and its applications, *J Tongji Univ, Shanghai* **22** (May 1994), 61–67.
[16] R.H. Scanlan and J.J. Tomko, Airfoil and bridge deck flutter derivatives, *J Eng Mech* **97** (1971), 1717–1737.
[17] M. Shinozuka and G. Deodatis, Simulation of multi-dimensional gaussian stochastic fields by spectral representation, *Applied Mechanics Reviews* **49**(1) (1996), 29–53.
[18] E. Simiu and R.H. Scanlan, *Wind effects on Structures*, John Wiley and Sons Inc, NY, 1986.
[19] S. Timoshenko, D.H. Young and W. Weaver, Jr, *Vibration Problems in Engineering*, J Wiley, NY, 1974.
[20] M.S. Troitsky, *Cable-Stayed Bridge – An Approach to Modern Bridge Design*, John Wiley and Sons Inc, NJ, 2003.
[21] Y.L. Xu and W.H. Guo, Dynamic analysis of coupled road vehicle and cable-stayed bridge systems under turbulent wind, *Journal of Engineering Structures* **25** (2003), 473–486.
[22] Y.L. Xu and W.H. Guo, Effects of bridge motion and crosswind on ride comfort of road vehicles, *J Wind Eng Ind Aerodyn* **92** (2004), 641–662.
[23] C. Yang, Seismic analysis of long span bridges including the effects of spatial variation of seismic waves on bridges, PhD Thesis, 2007, HKUST, HK.
[24] Y.B. Yang and B.H. Lin, Vehicle-bridge interaction analysis by dynamic condensation method, *J Struct Engrg, ASCE* **121**(11) (1995), 1636–1643.
[25] Y.B. Yang, D.J. Yau and Y.S. Wu, *Vehicle-Bridge Interaction Dynamics: With Applications to High-Speed Railways*, River Edge, NJ, 2001.